

Comparative Evaluation of Machine Learning Models for Predicting Donor Kidney Discard

Peer Schliephacke^{1†}, Hannah Schult^{1†}, Leon Mizera^{1†},
Judith Würfel^{1†}, Gunter Grieser², Axel Rahmel³,
Carl-Ludwig Fischer-Fröhlich³, Antje Jahn-Eimermacher^{1*}

^{1*}Department of Mathematics and Natural Sciences, Darmstadt University of Applied Sciences, Schöfferstraße 3, Darmstadt, 64295, Hessen, Germany.

²Department of Computer Science, Darmstadt University of Applied Sciences, Schöfferstraße 3, Darmstadt, 64295, Hessen, Germany.

³Deutsche Stiftung Organtransplantation, Deutschherrnufer 52, Frankfurt, 60594, Hessen, Germany.

*Corresponding author(s). E-mail(s): antje.jahn@h-da.de;

†These authors contributed equally to this work.

Abstract

A kidney transplant can improve the life expectancy and quality of life of patients with end-stage renal failure. Even more patients could be helped with a transplant if the rate of kidneys that are discarded and not transplanted could be reduced. Machine learning (ML) can support decision-making in this context by early identification of donor organs at high risk of discard, for instance to enable timely interventions to improve organ utilization such as rescue allocation. Although various ML models have been applied, their results are difficult to compare due to heterogenous datasets and differences in feature engineering and evaluation strategies. This study aims to provide a systematic and reproducible comparison of ML models for donor kidney discard prediction. We trained five commonly used ML models: Logistic Regression, Decision Tree, Random Forest, Gradient Boosting, and Deep Learning along with an ensemble model on data from 4,080 deceased donors (death determined by neurologic criteria) in Germany. A unified benchmarking framework was implemented, including standardized feature engineering and selection, and Bayesian hyperparameter optimization. Model performance was assessed for discrimination (MCC,

AUC, F1), calibration (Brier score), and explainability (SHAP). The ensemble achieved the highest discrimination performance (MCC=0.76, AUC=0.87, F1=0.90), while individual models such as Logistic Regression, Random Forest, and Deep Learning performed comparably and better than Decision Trees. Platt scaling improved calibration for tree-and neural network-based models. SHAP consistently identified donor age and renal markers as dominant predictors across models, reflecting clinical plausibility. This study demonstrates that consistent data preprocessing, feature selection, and evaluation can be more decisive for predictive success than the choice of the ML algorithm.

Keywords: Organ Transplantation, Donor Kidney Discard, Machine Learning, Calibration, Explainable AI, Feature Selection

1 Introduction

The global shortage of donor organs remains a significant challenge in modern medicine. While the demand for transplants continues to rise, organ donations fluctuate [1] and often fall short of clinical needs. At the same time, the quality of donor organs has declined, with increasing donor age and a reduced number of usable organs per donor [2]. These circumstances make allocation and acceptance decisions both highly complex and time-critical as preservation limits and ischemic-time related risks impose strict time constraints. As a consequence a substantial proportion of retrieved donor kidneys is ultimately discarded. Therefore, a research question of particular relevance in this context is the early identification of donor organs at high risk of being discarded, for instance to enable interventions to increase organ utilization such as timely rescue allocation efforts or applying machine perfusion to improve organ quality.

Machine learning (ML) models can support clinical decision-making by making use of the large volumes of available data, including biopsy reports, laboratory values, and free-text clinical records. Consequently, various ML models have been applied in the context of organ transplantation, often with promising results [3–8]. Thereby, kidney transplantation represents a frequently studied area due to the relatively large number of available cases. Commonly used ML models include Decision Trees (DT) and Regression Models as well as more flexible methods such as Random Forests (RF), Gradient Boosting, and artificial neural networks, which are generally less interpretable but may offer higher predictive performance. These models also have been applied to the specific task of predicting kidney discard risk, yielding heterogeneous results: Logistic regression (LR) remains one of the most commonly used approaches in this context, identifying key predictors associated with organ discard, such as biopsy findings and high Kidney Donor Profile Index scores [5, 9–13]. Some studies report improved predictive performance when using more advanced ML models, such as gradient boosting or RF [7, 14]. Other studies have found ML approaches to perform similarly to LR [15]. However, these studies are difficult to compare directly, as the underlying datasets vary substantially. For example, one study analyzed a large national dataset with several hundred predictors, whereas another relied on single-center data with a much smaller

sample size and a limited set of predictors. Furthermore, the role of feature selection [16] is often overlooked, potentially favoring models with built-in feature selection mechanisms such as RF. This makes it difficult to draw systematic conclusions about which models are most suitable for predicting kidney discard risk and thus supporting clinical decision-making in organ transplantation. The aim of this study was to address this gap by systematically comparing different ML approaches for predicting kidney discard risk, using a consistent preprocessing and transformation pipeline on a shared dataset of kidney transplantation candidates.

This work makes two main contributions. First, multiple state-of-the-art ML models are systematically evaluated with advanced techniques such as model calibration and Bayesian hyperparameter optimization applied to ensure an objective comparison. Second, not only prediction performance but also model explainability is compared through the use of SHAP, which enables the identification of key predictors and supports clinical interpretability.

Although the proprietary data used in this study cannot be shared because of confidentiality restrictions, we provide comprehensive access to all accompanying scripts for data processing, feature engineering and selection, model optimization, training, evaluation, calibration, and visualization to promote transparency and reproducibility.

The structure of this paper is as follows. Section 2 describes the data, the ML models, and feature engineering strategies, followed by an outline of the model evaluation methodology. Section 3 presents the results of the model comparison, including discrimination performance, model calibration and explainability. Finally, Section 4 concludes the paper and highlights directions for future work.

2 Methods

2.1 Data

Data on all kidneys offered for transplantation from deceased adult donors in Germany between April 2020 and August 2024 were used. The dataset, provided by the German Organ Procurement Organization (DSO), includes information from $n = 4080$ adult donors (all deaths determined by neurological criteria). Only donor-related characteristics are considered in predicting whether a kidney would be discarded, while recipient characteristics are intentionally excluded. This approach enables the identification of donor kidneys at high risk of discard based solely on information available at the time of the organ offer, prior to allocation to a specific recipient.

Donor data were provided by the German Organ Procurement Organization (DSO) as an independent research database for secondary analysis. All identifiers were removed, and only anonymized data are included. The dataset includes those data that the DSO is legally required to provide to the national transplantation registry under national transplantation law (TPG). The secondary analysis of these anonymized data was conducted in compliance with the transplantation law.

An organ is defined as discarded if it was offered for transplantation but ultimately not transplanted for any reason. Discard is considered at the donor level rather than the organ level to ensure independent observations and circumvent intra-individual correlations. In most cases (3,716 out of 4,080), both kidneys from a donor were either

transplanted or discarded, making a donor-level classification straightforward. In 364 cases, only one kidney was transplanted while the other was discarded. These cases are classified as “transplanted” at the donor level. In summary, 929 (22.8%) of all donors are classified as discarded and 3151 (77.2%) of all donors are classified as transplanted (i.e. not discarded). Note, that for a small number of donors, inconsistencies in kidney transplantation status were observed. Due to data anonymization, these inconsistencies could not be resolved, and the data were therefore analyzed as reported.

Donors providing multiple organs are not excluded as organ combinations do not interact with kidney discard. They may influence post-transplant function, which was however not the focus of this study.

The data comprises results from examinations of various body parts, information about any medication that had been prescribed, laboratory measurements from the domains of virology, pathology and microbiology as well as details on hospital stays and medical diagnoses including ICD-10 codes (International statistical classification of diseases and related health problems) [17]. In summary, $p=1128$ variables are available and were further processed in the feature engineering step (see section 2.2). A comprehensive description of the study cohort across all these variables is not feasible. Therefore, we extract the features that will later turn out to be most important for prediction and summarize them in Table 1.

The dataset was split based on donor id allocating 80% of donor ids to the training set and 20% to the test set to ensure independence between training and evaluation data. Feature Engineering was executed on both sets separately with thresholds calculated on only the training set and applied on the test set. Additionally, a fixed 10% subset of the training data was reserved as a dedicated validation set for final model training and calibration, ensuring strict separation from the held-out test set used for final evaluation.

2.2 Feature Engineering

In this section, we describe feature transformations including time series processing, redundancy reduction, encoding of categorical variables and imputation of missing values. Some additional transformations of specific features are described in Appendix B.

Variables were selected, extracted and engineered without prior filtering by medical advisors to avoid selection bias. Only in cases of uncertainty primary investigators consulted medical experts to ensure appropriate data standardization (e.g. donor urine output adjusted to body weight of donor and standard time interval as $ml/kg/h$). Secondary validation was performed by medical advisors to ensure that the data reflect real world scenarios in deceased organ donation procedures.

2.2.1 Feature Extraction from Time Series

Many of the laboratory measurements come in the form of time series. 49 variables were identified as time series. An additional 40 variables were not considered time series, as more than 50% of donors had only a single recorded value for these variables. For these we chose either the most recent or the first recorded value. We categorized the time

Table 1 Descriptive statistics of the most influential features as reported in Figure 6. Individual dummy variables from one-hot encoding were excluded, as they do not capture the full information of the original categorical variable.

Feature	All donors <i>N</i> = 4080	Transplanted <i>N</i> = 3151	Discarded <i>N</i> = 929
Variables originally reported:			
Age (years), median [IQR]	58.0 [46.0, 69.0]	56.0 [44.0, 66.0]	68.0 [56.0, 78.0]
Diuresis (<i>kg/24h/kg</i> (body weight)), median [IQR]	36.88 [24.21, 53.33]	38.55 [26.52, 57.1]	30.59 [15.06, 42.86]
Heparinoids administered, n (%)	3873 (94.9)	3128 (99.3)	745 (80.2)
Variables extracted from time series:			
eGFR_MDRD (<i>ml/min/1.73m²</i>), median [IQR]			
- minimum	69.69 [44.92, 95.12]	76.45 [53.84, 100.42]	39.48 [19.81, 66.8]
Creatinine (<i>g/l</i>), median [IQR]			
- Minimum	0.78 [0.6, 1.0]	0.72 [0.58, 0.9]	1.02 [0.77, 1.5]
- Maximum	97.2 [74.22, 141.61]	88.4 [70.7, 123.8]	154.7 [97.2, 291.7]
- Intercept	81.58 [61.93, 116.02]	75.92 [59.47, 101.44]	118.88 [84.0, 197.31]
- Last	79.6 [61.9, 114.9]	75.1 [59.2, 99.0]	118.5 [79.6, 193.6]
- Standard deviation	11.22 [5.79, 22.55]	10.3 [5.36, 18.8]	19.59 [7.47, 59.77]
Nitrite, median [IQR]			
- Count	1.0 [1.0, 1.33]	1.0 [1.0, 1.32]	1.0 [1.0, 1.33]
Urea (<i>mmol/l</i>), median [IQR]			
- Minimum	4.3 [3.0, 5.9]	4.0 [2.8, 5.3]	5.9 [4.2, 8.0]
- Maximum	7.0 [5.0, 10.0]	6.3 [4.7, 9.0]	9.9 [6.8, 16.3]
Blood gases FIO2 (1/1), median [IQR]			
- First	0.51 [0.4, 0.7]	0.51 [0.4, 0.79]	0.54 [0.4, 0.68]
Blood gases pH, median [IQR]			
- Count	2.0 [1.0, 3.0]	2.0 [1.0, 3.0]	2.0 [1.0, 2.34]
Potassium (<i>mmol/l</i>), median [IQR]			
- Maximum	4.5 [4.2, 4.9]	4.5 [4.2, 4.9]	4.7 [4.4, 5.2]
INR (1/1), median [IQR]			
- First	1.1 [1.01, 1.25]	1.1 [1.0, 1.23]	1.14 [1.05, 1.3]
Nitrite negative, n (%)			
- First	3499 (85.8)	2830 (89.8)	669 (72.0)
Glucose negative, n (%)			
- First	2928 (71.8)	2392 (75.9)	536 (57.7)
Protein qualitative negative, n (%)			
- First	2069 (50.7)	1772 (56.2)	297 (32.0)
Protein qualitative negative, n (%)			
- First	2082 (51.0)	1790 (56.8)	292 (31.4)

series variables into the following subtypes to maximize the extracted information for each variable:

- Type 1: Time series variables with categorical values, that indicate a positive or negative outcome only.
- Type 2: Time series variables with numerical values and a mean number of observations per donor lower than two.
- Type 3: Time series variables with numerical values and a mean number of observations per donor of two or more.

For each time series variable, we extracted the following features for every donor: the first recorded value, the last recorded value, the number of entries, and the time span between the first and last entry (measured in hours).

For time series variables with numerical values (type 2 and 3) we also extracted the standard deviation, minimum, and maximum values.

For time series variables of type 3, we further extracted features describing the linear trend over time: A linear regression per donor was performed modeling the value of the variable (dependent variable) over time measured in hours since the first entry (independent variable). Thus, the linear regression model for every donor d is:

$$y_{d,i} = \beta_{d,0} + \beta_{d,1} \cdot t_i + \varepsilon_{d,i} \quad (1)$$

where $y_{d,i}$ denotes the value of the variable at the time point t_i . The estimated coefficients $\hat{\beta}_{d,0}$ and $\hat{\beta}_{d,1}$ were used as additional features.

Previous studies use the last recorded value [18] or the minimum value [18, 19]. Our additionally extracted features may capture changes over time: The number of entries may indicate that variable values for a donor have changed over time. Similarly, the time span between the first and last entry can also reflect temporal dynamics in the donor’s condition. The standard deviation also provides insights into the level of variability. The estimated linear regression coefficients include information on whether the values generally increased or decreased over time and to what extent. In summary, a total of 364 features were extracted from the time series data.

2.2.2 Feature Extraction from Donor Medication Data

In the raw data there are 1772 unique medication names. These are structured such that the first word describes the medication and the remaining ones give additional information such as dosage. Considering only the first word of each medication entry reduced the number of medication names to 1103. Afterwards, the 40 most frequent medication names were selected for the final feature set. This selection captures approximately 80% of all medication administrations in the dataset. They were turned into binary features indicating, whether a donor had taken the medication or not.

2.2.3 Categorical Variable Encoding

We used One-Hot encoding for categorical variables with more than two values. Thereby, for variables containing ICD-10 codes, we replaced codes with a relative frequency of less than 1% of donors in the training set by missing values.

2.2.4 Missing Value Imputation

Approximately 14% of the values in our data are missing with 628 of the variables having incomplete data. These were imputed in the same way in training and test set unless stated otherwise as follows:

- 250 variables could be imputed using logical dependencies following expert advice. These include variables on certain diagnoses where a missing value can be interpreted as a negative value (i.e. no diagnosis present).
- For some categorical variables missing values were kept and considered a separate category. These are variables where a missing value is considered to potentially influence the decision about discard (e.g. 'urine_glucose').
- For two variables ('CPR duration' and 'ecmo') free text variables provided additional information and were used for imputation.

- 30 continuous variables describing physiological parameters were imputed with random samples from a normal distribution with mean and standard deviation of each variable, retaining only values from within the central 95% range of this distribution. The distribution was calculated separately for training and test set.
- For 20 variables with a high percentage of missing values (>70%) in the training set the specific values were dropped and the variables dichotomized into "missing" and "not missing". In these cases imputation based on sparse data was considered unreliable and therefore not performed.
- The remaining 328 variables with missing values in the training set were imputed with an iterative imputing algorithm [20] using ridge regression to predict the missing values for both training and test set. If there were variables with missing values in the test set that had no missing values in the training set, these were filled with the mean of that variable. This method was chosen to account for complex relationships between variables.

Finally, we evaluated the result of this imputation strategy using a Histogram-based Gradient Boosting Classification Tree. The HistGradientBoostingClassifier has an intrinsic method for imputing missing values [21] and results relying on this method can be compared to results with prior imputation using our imputation strategy. We trained a HistGradientBoostingClassifier on the training set of both the final imputed feature set as well as the original version without imputation using a grid search and five-fold cross-validation. Performance on the test set (F1 score and MCC) was compared. The scores relying on our imputation strategy were superior to those of the intrinsic strategy of the HistGradientBoostingClassifier, indicating a successful imputation strategy.

2.3 Modeling Approach

The following section outlines our modeling approach, including the ML algorithms, feature selection techniques, and hyperparameter optimization methods applied to the kidney transplantation dataset.

2.3.1 Machine Learning Algorithms

The following ML algorithms are trained to predict the probabilities of donor organs being either discarded or transplanted.

Decision Trees

Decision Trees (DTs) [22] are supervised learning models used for classification and regression tasks. They split data recursively into subsets based on feature thresholds, forming a tree-like structure where each internal node represents a decision and each leaf node provides a final prediction. DTs are known for their interpretability, as each split is based on simple rules derived from an impurity measure such as the Gini impurity, but are prone to overfitting [22], especially when the tree is deep.

Logistic Regression

Logistic Regression (LR) [23] is a ML algorithm from the linear family, commonly used for binary classification tasks. LR models the probability of an outcome by applying a sigmoid function (logistic) to a linear combination of input features. The regression model usually uses the least squares method to find the parameters for each feature which minimize the sum of squared errors regarding the target variable [23]. An additional advantage is its interpretability, since feature importance can be directly inferred from the model coefficients.

Random Forest

Random Forest (RF) [24] is an ensemble learning method that builds multiple DTs and combines their outputs to improve predictive accuracy and decrease overfitting. The forest model uses the bagging method by training each tree on a random subset of the data and features resulting in reduced overfitting compared to individual DTs. An additional advantage is the possibility to derive aggregated feature importance measures across all trees, which enhances interpretability.

eXtreme Gradient Boosting

Extreme Gradient Boosting (XGB) [25] is an ensemble learning algorithm based on gradient boosting [26], suitable for classification and regression tasks. The model builds DTs sequentially, where each new tree corrects the errors of the previous ones, optimizing performance through gradient descent. XGB performs especially well on structured data [27] and can even outperform deep learning algorithms [28]. An additional advantage is the availability of feature importance measures which provide interpretability despite the model's complexity.

Multilayer Perceptron

Multilayer Perceptron (MLP) (also known as Deep Learning) [29] is an artificial neural network used for both classification and regression tasks. It consists of multiple layers of interconnected neurons, including an input layer, one or more hidden layers and an output layer, where each neuron applies a weighted sum of inputs followed by a nonlinear activation function. MLPs are capable of capturing complex, nonlinear relationships but require careful tuning of hyperparameters and large datasets to generalize well. Although they are more commonly applied to unstructured data such as images or text, MLPs can also be used on structured tabular data.

Ensemble

An ensemble model, referred to as the data ensemble model (DE), was implemented to combine the predictions of several pretrained classifiers. In this study the DE integrates the outputs of LR, XGB, RF and MLP. Each model produces a probability for both classes and the ensemble aggregates these outputs by computing the mean of the predicted probabilities across models. The final classification result is determined by selecting the class with the highest averaged probability. Decision Trees were

excluded from the ensemble due to their comparatively lower performance, as will be demonstrated in later sections.

2.3.2 Feature Selection

To address the high dimensionality of our dataset, we apply a feature selection approach to identify the most promising subset of features. This reduces redundancy, improves model interpretability, and prevents overfitting by focusing on the variables most relevant to prediction [16]. Because different machine learning models capture relationships in distinct ways, we perform the feature selection separately for each model but always with the same method. This ensures that each algorithm operates on a feature set tailored to its specific inductive biases and complexity. To capture nonlinear and multivariate interactions between features, we employ an optimization method based on genetic algorithms [30] with their ability to navigate large search spaces [31]. This approach can uncover complex relationships that simpler univariate filters (e.g., correlation or chi-square tests) may miss [32, 33].

The general approach is applied separately for each ML model as depicted in Figure 1 and described in the following.

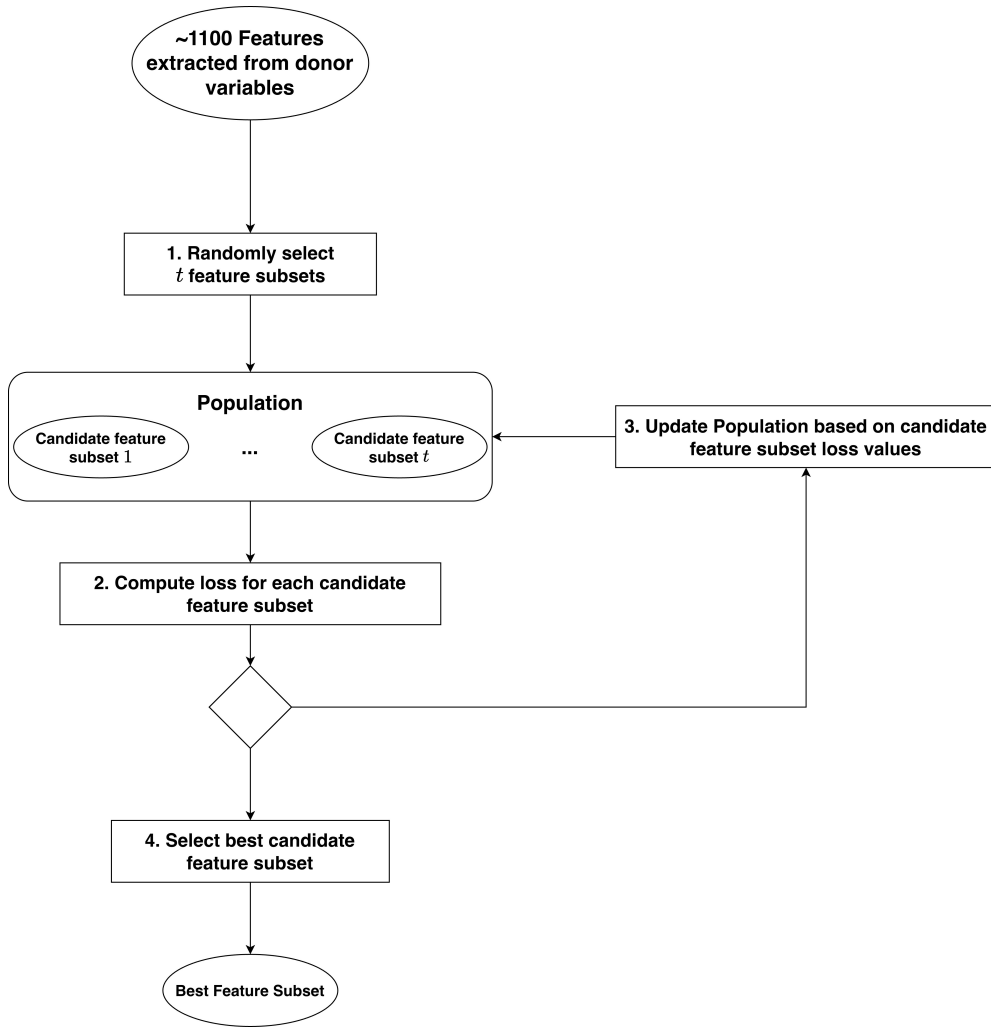


Fig. 1 Schema of the feature selection process. Starting from the full feature space, multiple candidate feature subsets are created and evaluated by training and validating a supervised model. Each subset is assigned a loss value based on its predictive performance, and the subset with the smallest loss is selected as the final feature subset.

We use the Nondominated Sorting Genetic Algorithm II (NSGA-II) [34] for single-objective feature selection optimization, as it natively handles binary and categorical parameters, unlike other evolutionary strategies [35]. We use the optuna [36] implementation for the NSGA-II algorithm.

1. First, a population of 50 randomly selected feature subsets are selected as candidates. Feature sets here are represented as boolean vector of length ~ 1100 (number

of features in the feature set) where each element represents a feature and is set to either one or zero depending whether the feature is included in the subset or not.

2. Next, for each feature subset, we train the machine learning algorithm under investigation using only the corresponding features and evaluate its performance in terms of loss metrics. The procedure for computing these performance measures is described in more detail below:
 - We perform a nested hyperparameter optimization to build the model architecture: For each candidate feature subset we run a randomized hyperparameter search [37] with 10 trials to avoid overfitting of the default model hyperparameters to a specific feature subset. For each of these 10 trials we evaluate the generated model configuration with 3-fold cross-validation, where we train and validate the ML algorithm.
 - The yielded validation loss from the 3-fold cross-validation is calculated using the normed normed Matthews Correlation Coefficient (MCC, See also section 2.4.1) [38], a balanced metric that combines true/false positives/negatives into a single correlation score, since the MCC provides a more informative assessment than other common metrics for imbalanced settings [39, 40].
 - The overall loss for a subset is defined as the mean of the 10×3 validation losses produced by the inner search plus an explicit penalty term on feature count namely $\lambda \cdot n_{\text{features}}$ (with $\lambda = 0.0005$) to discourage the selection of large redundant feature subsets.
3. Finally, the best performing feature subsets are selected and form the basis for evolutionary operations (selection, crossover, and mutation) which yield a next generation of the population of feature subsets. For these, the process is repeated.
4. After 1000 iterations, the process terminates, yielding the best-performing feature subset as the result for each ML algorithm, respectively.

Our approach follows prior work in related domains but differs in the use of multi-objective evolutionary search per model and the nested randomized-architecture evaluation strategy, which together aim to produce robust, compact feature sets tailored to each classifier rather than a single global subset [41, 42].

Additionally 93 features that were redundant or constant after imputation were dropped.

2.3.3 Model Hyperparameter Optimization

The feature selection produced five optimized feature subsets, one tailored to each ML model. To identify the best architecture for each algorithm, we then perform a dedicated hyperparameter optimization on the corresponding optimized feature space.

We use optuna with the Tree-structured Parzen Estimator (TPE) sampler [43] as a Bayesian hyperparameter strategy [44] to identify the best hyperparameter configurations for each ML algorithm. The optimization objective was the mean 5-fold cross-validation normed MCC. For each algorithm we ran 300 trials where the corresponding hyperparameter search spaces are listed in Tables C1-C5 and the selected (best) architectures are reported in Tables C6-C10.

2.4 Model Evaluation

The following sections present the concrete evaluation steps of our model evaluation. We first report how we assess discrimination performance, including statistical comparisons between models, then present methods for calibration analyses on predicted probabilities, and finally summarize how we get explainability findings using SHAP-based attributions.

2.4.1 Discrimination Performance

For final performance assessment we retrain each selected hyperparameter configuration using 30 different random seeds to quantify variability following recommended practice [45–47].

Thus, the random seeds control sources of stochasticity inherent to the learning algorithms, promoting reproducibility and enabling assessment of performance variability due to random initialization effects. For DT, randomness may affect feature-threshold selection when multiple candidates yield equal impurity reductions. In LR, using the saga solver [48], stochasticity arises from the sampling of data subsets during iterative optimization. In ensemble based methods such as RF, the random seed governs the bootstrapping of training samples and random feature selection at each split, directly affecting tree diversity and thus overall model variance [49]. Similarly, in XGB, seeds define the stochastic elements in subsampling of rows and columns used for constructing individual trees, influencing the bias variance trade off. Finally, for the MLP, seeds determine the initialization of network weights and biases as well as the mini batches during training, both of which can substantially influence convergence and final performance [50–52]. Retraining each model under multiple random seeds captures the distribution of attainable performances and quantifies the inherent stability or variability of each algorithm beyond single-run performance estimates.

Retraining was conducted using the original train–validation split, comprising 90% of the data for training and 10% for validation, determined via a random split. Feature standardization was performed using z-score scaling, with the scaling parameters (mean and standard deviation of the respective feature) computed exclusively on the training set and subsequently applied to both the validation and test sets to prevent information leakage. Model performance was evaluated on a held-out test set that was not utilized during training or validation.

We report three complementary performance metrics for each seed run: F1 score (See Equation 2 [53]), Area Under the ROC Curve (AUC) [54], and MCC (See Equations 3 and 4 [39, 40]). In Equations 2–4, TP, TN, FP, and FN denote the counts of true positives, true negatives, false positives, and false negatives. Respectively, in the context of donor kidney acceptance, a true positive (negative) corresponds to a kidney correctly predicted as transplanted (discarded), and vice versa for false positives and false negatives. Metrics are collected across all seeded runs and reported as distributions rather than single-point estimates to visualize variability of each algorithm.

The F1 score (range 0–1), the harmonic mean of precision (also known as positive predictive value) and recall (also known as sensitivity), focuses on positive-class performance but fails to account for true negatives and therefore can be misleading under class imbalance [39]. The AUC measures the classifier’s ability to assign a higher probability of successful transplantation to a randomly chosen transplanted organ compared to a randomly chosen discarded organ (range 0–1, where 0.5 indicates random performance), but it can be overly optimistic for small or imbalanced datasets [55, 56]. For those reasons, we emphasize the MCC metric because it provides a more informative assessment for imbalanced binary classification as it captures all four confusion matrix components and yields a balanced measure even when class sizes differ [39, 40].

To determine whether observed differences among models are statistically significant we first apply an Analysis of Variance (ANOVA) [57] followed by Tukey’s Honest Significant Difference (HSD) post-hoc test [58] for pairwise model comparisons.

$$F_1 = \frac{2 \cdot TP}{2 \cdot TP + FP + FN} \quad (2)$$

$$MCC = \frac{TP \cdot TN - FP \cdot FN}{\sqrt{(TP + FP)(TP + FN)(TN + FP)(TN + FN)}} \quad (3)$$

$$MCC_{Normed} = \frac{MCC + 1}{2} \quad (4)$$

2.4.2 Model Calibration

Model calibration is essential in the clinical domain because well-calibrated probabilities convey reliable predictive uncertainty and support safer decision-making [59–61]. We quantify calibration using the Brier score [62, 63], defined as the mean squared error between predicted probabilities and true binary outcomes (range 0–1 where lower is better) [64, 65].

Post-hoc calibration adjusts a trained model’s predicted probabilities to better match the true outcome frequencies, improving the reliability of its probability estimates.

Specifically, post-calibration methods transform the raw prediction scores such as the uncalibrated outputs of a classifier like the decision function or pre-sigmoid logits into well-calibrated probability estimates. We compare two standard post-calibration approaches. Platt scaling [66] fits a parametric sigmoid function (a two-parameter logistic model, commonly implemented as LR) that maps these scores to probabilities. Its parameters are optimized on the validation data and then applied to the test predictions. Isotonic regression [67], in contrast, provides a non-parametric monotonic mapping capable of modeling more complex distortions between raw scores and true probabilities. In our setup, each calibrator is trained separately for each model on the validation predictions (using default hyperparameters for the calibration model), applied to the test set, and evaluated using the Brier score as well as reliability plots to visualize residual miscalibration.

Note that we excluded the DE model from the post-calibration analyses because each base model was trained on a different feature subset. As a result, post-hoc

calibration methods cannot operate on the combined predictions. Furthermore, the calibration results are not aggregated over the 30 different random seeds from the final re-training, as there is no straightforward way to combine calibration plots. Instead, only the results corresponding to the best test run are shown. While this may lead to slightly overoptimistic calibration estimates, the main objective (model comparison) is not affected, as it applies to all models.

2.4.3 Explainability

To evaluate explainability we used SHAP [68] as a model-agnostic method that uniformly apply across different model families. SHAP is grounded in Shapley values [69] from cooperative game theory. For each observations the contributions of each feature to the difference between the predicted risk and the marginal (average) population risk are calculated. Thus, the contributions of all features sum to the model output deviation from the baseline (expected) prediction. This additive property makes SHAP suitable for both local (per-instance) and aggregated global interpretation. Here, we focus on global interpretation for model comparison by aggregating SHAP values per feature across all observations. Aggregation is performed using absolute SHAP values since, for global feature importance, the magnitude rather than the sign is relevant. Each feature is summarized by its mean absolute SHAP value, with the corresponding standard deviation to reflect variability across samples and runs. In addition, for detailed model analysis, we also examine individual explainability results to capture instance-level behavior via beeswarm plots.

SHAP has been widely applied in tabular and clinical ML studies to highlight predictive drivers and support clinician interpretation [70–72] and specifically to improve transparency in medical prediction tasks [61].

In individual studies where model comparison is not the main focus, model-specific explainers may be used as suitable tools for interpreting the results. We therefore complemented results of SHAP by model-specific explainability methods (e.g., decision-tree feature importances, linear model coefficients) which can be biased due to overfitting and do not uniformly apply across the used model families [73–75].

We implement SHAP using the same explainer object (Permutation), as SHAP is a model-agnostic framework for explainability. The training dataset is used as background data, and the model’s output probabilities serve as the link function between SHAP and the algorithm.

Analogous to the post-calibration of the DE model, SHAP cannot be applied because feature attributions across heterogeneous feature sets are not comparable. Moreover, we report SHAP values and plots only for the best-performing test run, as aggregating feature attributions across multiple random seeds would not yield meaningful or interpretable results.

3 Results

In this section, we first present and discuss the discrimination performance of all models. Then we analyze their probability calibration before concluding with an assessment of model explainability.

3.1 Discrimination Performance

Table 2 presents the test performance scores aggregated from the final re-training and evaluation runs. The DE outperforms all other models across every performance metric, with particularly large gains in AUC and F1 score. In contrast, the differences in normed MCC between DE, MLP, and LR are comparatively smaller.

Table 2 Performance scores defined in Section 2.4.1 for each of the six evaluated models: DT, LR, RF, XGB, MLP, and DE. Values represent mean test performance in terms of F1 score, AUC, and normalized MCC. The best performance scores are highlighted with a bold font.

Model	F1	AUC	Normed MCC
DT	0.7336	0.6892	0.6219
LR	0.8192	0.8564	0.7515
RF	0.8136	0.8420	0.7334
XGB	0.7985	0.8219	0.7119
MLP	0.8279	0.8499	0.7550
DE	0.9042	0.8721	0.7588

Figure 2 (left) shows the model performance distribution using the normed test MCC across the different random seeds: DT performs worst, while the XGB is second lowest but stronger compared to the DT model. The DE scores significantly best, while RF, MLP, and LR perform comparably to the ensemble with no significant difference according to the Tukey-HSD post-hoc test. The adjusted pairwise Tukey p-values are shown in Figure 2 (right) with colors indicating statistical significance.

Appendix Figure D1 shows the respective performance plot for the test F1 score, while Appendix Figure D2 shows the performance plot for the test AUC score. The ranking of top-performing models remains consistent. The ensemble achieves a significantly higher F1 score than all others. For the test AUC, the ensemble also ranks first, with only LR being not statistically significantly inferior. The DT model achieves a much lower performance for all three scores.

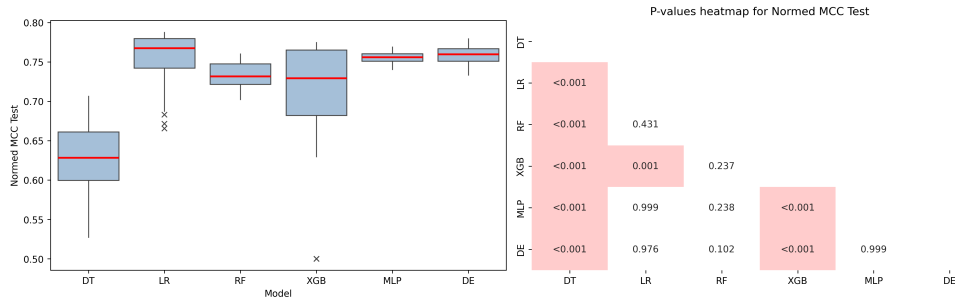


Fig. 2 Left: Discrimination performance evaluation of six different ML models. Each panel reports the normed test MCC (Y-axis, higher is better) for multiple approaches: XDT, LR, RF, XGB, MLP, and DE. Boxplots show the performance distribution for each method. **Right:** Lower-triangle heatmap of Tukey-adjusted p-values showing pairwise statistical significance between models.

The DT performs worst in our experiments, which aligns with prior findings on clinical tabular data [76, 77]. A single tree often lacks the capacity required for complex patterns and is vulnerable to overfitting [78].

The ensemble model is consistently the best performing approach for each test metric, in line with evidence that ensembles reduce variance and improve scoring accuracy [4, 79, 80]. In our setting this advantage is amplified because each base model is trained on a data space tailored to its model family through feature selection. This diversification lowers error correlation and strengthens the combined prediction.

The ensemble shows the largest gains on F1 and AUC, while the gap on MCC is smaller. This suggests that MCC is a more demanding and informative metric in our context. The competitive MCC scores of RF, MLP, and LR indicate that the preceding feature selection and hyperparameter optimization were effective.

3.2 Model Calibration

Table 3 reports Brier scores, comparing probability calibration across three methods for each model: no post-calibration, post-calibration using Platt scaling, and post-calibration using isotonic scaling. Lower values indicate better calibrated probabilities. In this dataset, Platt scaling yields the lowest Brier scores for DT, RF, and MLP, while the uncalibrated versions of LR and XGB perform best. Notably, LR without any post-calibration method achieves the best brier score overall.

The respective calibration curves [81] can be found in Figures 3 and 4 showing models without post-calibration and with post-calibration using Platt scaling. The legend reports Brier Scores (lower is better). The dashed diagonal indicates perfect calibration. The calibration curves for isotonic scaling are not shown here as this method appeared to be generally inferior (see Appendix Figure E3). X-axis reports predicted probability and Y-axis reports the empirical probability (observed fraction of positives) within each probability bin. Figure 4 shows improved calibration for DT, RF, and MLP, with reliability curves closer to the ideal diagonal.

Table 3 Calibration performance of different algorithms measured by the Brier score.

Algorithm	Without Post-Calibration	With Post-Calibration	
		Platt Scaling	Isotonic Scaling
DT	0.1453	0.1412	0.1419
LR	0.1023	0.1036	0.1082
RF	0.1291	0.1171	0.1248
XGB	0.1137	0.1154	0.1204
MLP	0.1344	0.1190	0.1203

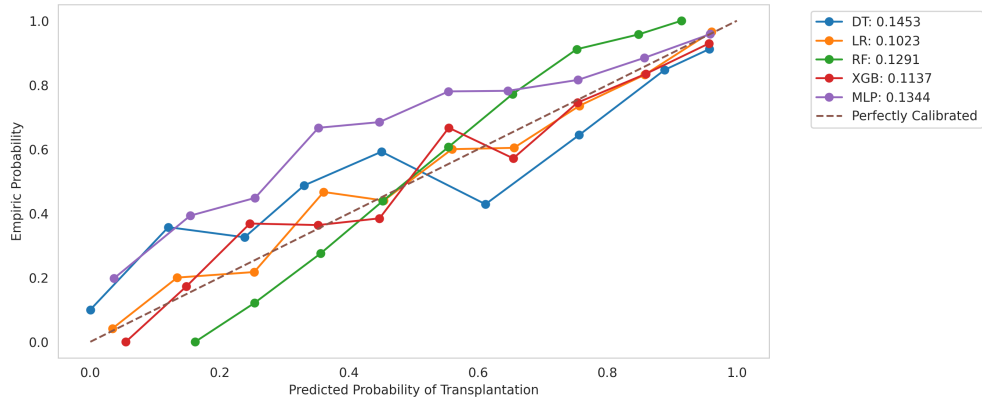


Fig. 3 Calibration curves without post-calibration for DT, RF, LR, XGB, and MLP.

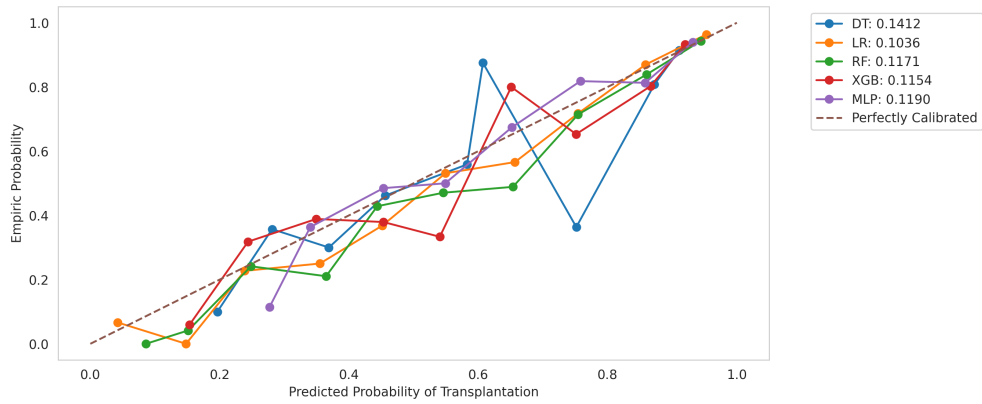


Fig. 4 Calibration curves for platt post-calibration for DT, RF, LR, XGB, and MLP.

Across models, Platt scaling yields more reliable probability calibration than isotonic scaling. However, the need of post-calibration is model dependent: LR and XGB are already well calibrated without calibration and show little or no benefit, whereas DT, RF, and MLP benefit more from Platt scaling. This observation aligns with prior knowledge since LR models are often well calibrated by default since the loss is optimized with the canonical logit link aligning predicted probabilities with true observations [82]. DT and RF are expected to have poor Brier scores if uncalibrated because they can produce overconfident probability estimates, particularly in cases where the training data is limited or imbalanced, leading to misalignment between predicted probabilities and actual outcomes [83]. Similarly, MLPs are expected to be poorly calibrated, most likely due to overfitting caused by the large number of parameters, which is why the benefits of calibration techniques are anticipated [84].

3.3 Explainability

Detailed SHAP beeswarm plots [68] show the most important features depending on background data predictions. These visualizations display per-sample SHAP values (showing the direction and magnitude of a feature’s effect on the prediction), the dispersion of contributions across the cohort, and how contributions vary with the original feature values (color scale), thereby highlighting potential interactions and outliers. Figure 5 illustrates this for the example of LR (See Appendix F for the other algorithm types).

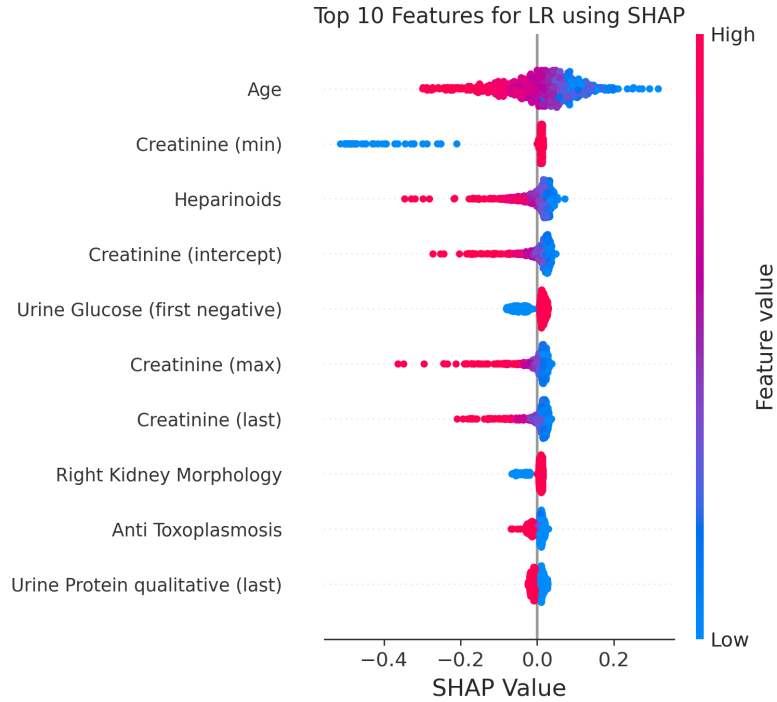


Fig. 5 Beeswarm plot of SHAP values showing the distribution and impact of features on LR donor transplantation predictions. Each point represents an individual instance (test set), positioned by its SHAP value and colored by the feature’s actual value, illustrating both the magnitude and direction of feature influence. Top features include age, time-series aggregates of renal function measures and medication information.

To compare the results on explainability between the six different models we aggregate SHAP values such as shown in Figure 5 to a single value using the mean value. Figure 6 reports the aggregated importance of the ten most influential features per model. Notably, several features consistently align among the top contributors, frequently exhibiting the largest SHAP magnitudes for example, Age, heparinoids (heparinoid medication), and time-series information related to renal function such as creatinine, urea values, and eGFR. The features consistently identified as most important for kidney acceptance prediction align with domain expectations and prior work across different ML models. These include Age, renal function measures such as eGFR, creatinine, and urea, pH and other blood gas values, and aggregated urinary information [4, 61, 85, 86]. The high apparent importance of heparinoid medication should be interpreted with caution, as in the majority of cases it was administered intravenously immediately prior to organ retrieval as part of the standard donation procedure. Thus, its high importance may partly reflect its association with successful organ procurement rather than a true prognostic effect.

Top 10 important Features based on absolute SHAP Values

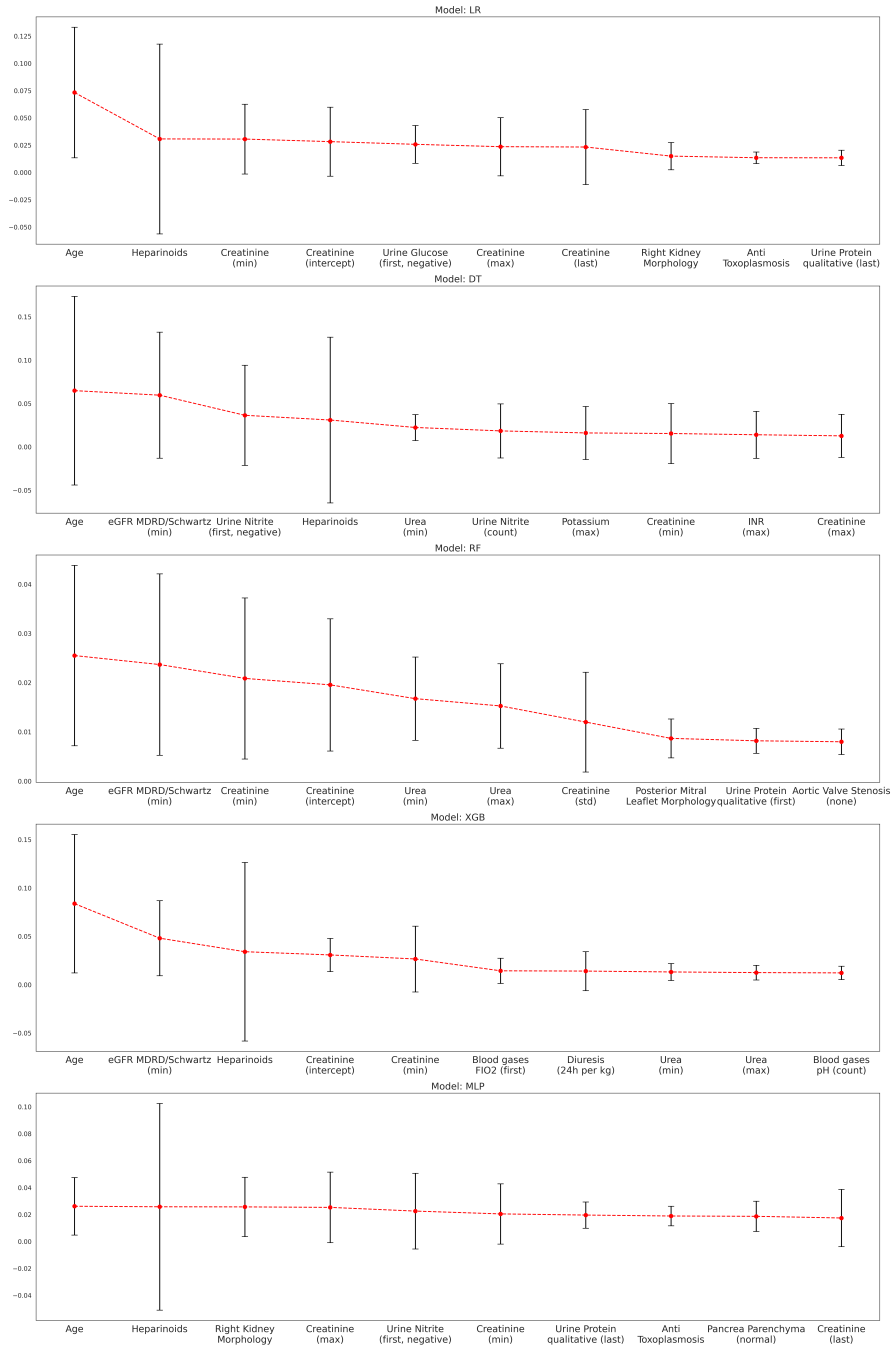


Fig. 6 Top 10 features by mean absolute SHAP value (with standard deviation) across five models (DT, LR, RF, XGB, MLP). Age (Alter) and renal function markers (eGFR, Kreatinin, Harnstoff) dominate model influence, with smaller, model-specific contributions from additional clinical variables. Suffixes such as "min value", "value count", "max value", "intercept", "first value negative", "last value", "std deviation", "qualitativ first value" correspond to aggregation features from time series for labor variables.

Despite not useful for model comparison, we also present model specific explainability plots in the Appendix F. Across models, global feature importance derived from SHAP broadly overlapped with model-specific explainability (See Appendix Figures F4-F10). However, the degree of overlap varied across algorithms, and the feature rankings differed between the two methods, indicating that the extent and consistency of shared important features depend on the underlying model.

4 Discussion

Our results base on a concise, transferable benchmarking procedure. First, we standardize data handling and feature construction from donor data: domain-aware imputation, feature extraction from time-series, and the encoding of donor medication data. Second, we perform per-model, supervised feature selection with NSGA-II to jointly optimize predictive performance (normed MCC) and parsimony, coupled with nested hyperparameter evaluation to reduce overfitting, followed by Bayesian TPE tuning on the tailored spaces. Third, we emphasize robust, comparable evaluation: seeded retraining with distributional reporting for MCC, F1, and AUC and repeated-measures ANOVA with Tukey HSD for fair model comparisons. Fourth, we calibrate probabilities when needed, using Brier score and reliability plots to choose between Platt and isotonic mappings trained on validation predictions and then applied to held-out test sets. Finally, we unify interpretation across model families with SHAP to provide signed, per-sample attributions and aggregated global importance, noting its assumptions and complementing it with model-specific diagnostics.

Although deep learning has shown superior performance over classical ML in many domains [87, 88], this advantage was not evident in our study, where LR and RF performed comparably to the MLP. This finding likely reflects the characteristics of our dataset which is moderate in size and tabular in structure limiting the capacity of deep learning models to exploit their full representational power [28, 89]. In such settings, simpler models like LR offer competitive predictive accuracy while maintaining interpretability and lower computational demands, making them attractive for clinical implementation.

Our results also highlight the importance of metric selection. Commonly reported metrics such as F1 and AUC may overestimate model performance, as they either ignore true negatives or fail to account for positive and negative predictive values. [39]. We therefore recommend using the Matthews Correlation Coefficient (MCC) as the primary evaluation metric for imbalanced clinical datasets, as it incorporates all four confusion matrix components and provides a more balanced measure of discrimination [40].

Contrary to prior reports suggesting isotonic regression as the superior post-calibration method [83], our analysis showed that Platt scaling achieved better calibration, particularly for tree-based and neural network models. The relatively small differences in Brier scores indicate that the models were already well calibrated, likely due to rigorous feature selection and hyperparameter optimization. We thus recommend applying calibration selectively, guided by model type and validated using reliability plots, with Platt scaling preferred for small datasets.

Finally, model interpretability remains a critical consideration for clinical adoption. Comparing model-agnostic and model-specific approaches reveals complementary strengths and limitations. Model-specific feature importances reflect algorithmic biases (e.g., regression coefficients or impurity-based scores), while SHAP offers a unified importance scale across model families [90, 91]. However, SHAP attributions can be influenced by feature correlation, background data, and independence assumptions, and aggregation of absolute SHAP values omits directionality. Furthermore, SHAP values can reflect associations but cannot distinguish underlying causal mechanisms as seen in the high importance assigned to heparinoid medication. Despite these constraints, SHAP proved valuable for identifying consistent, clinically plausible predictors and enabling local interpretability at the donor level which is an advantage over global feature rankings [68, 74]. Nevertheless, SHAP analyses should be interpreted in conjunction with model diagnostics and expert clinical judgment.

5 Conclusion

Given the abundance of models and heterogeneous clinical datasets, different ML models have been applied to predict the risk of donor discard, yet without a definitive conclusion on which model performs best [7, 14, 15]. Our systematic comparison using the same dataset provides more conclusive insights: An ensemble combining different model families achieves the highest discriminative performance, but comes with limitations regarding prediction derivation, calibration assessment, and explainability. Among individual models, which do not share these disadvantages, the MLP outperformed tree-based ensembles (e.g., RF, XGB). Somewhat unexpectedly, a simple linear additive model (LR) performed comparably well. This supports the continued widespread use of the well-explainable LR model [5, 9–13], and aligns with the findings of Sageshima et al. [15] who also reported similar performance between LR and other ML models. Importantly, explainability is not limited to linear models but can also be derived from more complex models by the use of SHAP values. We found SHAP to consistently identify known clinical drivers (e.g., age, renal function markers) across model families, supporting coherent interpretation. As expected, a single decision tree shows clearly inferior performance, likely due to its limited capacity to capture the complexity of the data.

Our results base on a concise, transferable benchmarking procedure that prioritizes methodology over single-number outcomes. In summary, our results highlight that methodological rigor and data preprocessing are more critical to predictive success with respect to donor discard than the specific choice of model type.

Declarations

Funding. The research project was funded by the Federal Ministry of Education and Research (project 13FH019KX1). The results presented in this article are the responsibility of the authors. The publication fees were funded by Darmstadt University of Applied Sciences.

Conflict of Interest/Competing interests. The authors declare no potential conflicts of interest with respect to the research, authorship, and/or publication of this article.

Ethics approval and consent to participate. The data were provided by the German Organ Procurement Organization (DSO) as an independent research database for secondary analysis. All identifiers were removed, and only anonymized data are included. The analysis of these anonymized patient data is permitted under §14 and §15 of the Transplantation Act (Transplantationsgesetz, BGBl. I S. 2206). Informed consent was not required according to §14 of the Transplantation Act (Transplantationsgesetz, BGBl. I S. 2206) as only retrospective and anonymized data from deceased organ donors were used. Medical ethical approval was not required according to §15 of the Professional Code of Conduct of the State Medical Association of Hesse as only retrospective and anonymized data of deceased organ donors were used. The research was conducted in accordance with the Declaration of Helsinki.

Consent for publication. Not applicable

Data availability. The analyses presented in this article are based on retrospective and anonymized data from the German Organ Procurement Organization (DSO). Due to data protection and institutional restrictions, these data cannot be made publicly available.

Materials availability. Not applicable

Code availability. An implementation of the applied analysis methods is available on <https://github.com/PeerHan/donor-kidney-discard-prediction>.

Author contribution. Axel Rahmel, Antje Jahn, and Gunter Grieser conceived and designed the study and planned the analyses; Peer Schliephacke, Hannah Schult, Leon Mizera, and Judith Würfel designed the feature engineering and performed all analyses, with medical guidance from Carl-Ludwig Fischer-Fröhlich. Peer Schliephacke drafted the first version of the manuscript. All authors reviewed, edited, and approved the final manuscript.

Acknowledgements. We gratefully recognize and appreciate the support and contributions of Thomas La Rocca (DSO) and Lukas Klein, Adrian Füller, Anika Fuchs, Danilo Zähle, David Heiß, Friedrich Heitzer, Katharina Litzinger, Kevin Saliu, Leonard Holdau, and Tristan Funk (h_da) to this work.

References

- [1] Organtransplantation, D.S.: Jahresbericht: Organspende und Transplantation in Deutschland (2023). <https://dso.de/SiteCollectionDocuments/DSO-Jahresbericht%202023.pdf> Accessed 2025-03-19
- [2] Yoon, J., Alaa, A.M., Cadeiras, M., Schaar, M.v.d.: Personalized Donor-Recipient Matching for Organ Transplantation. arXiv. arXiv:1611.03934 [cs] (2016). <https://doi.org/10.48550/arXiv.1611.03934> . <http://arxiv.org/abs/1611.03934> Accessed 2025-03-20

- [3] Shaikhina, T., Lowe, D., Daga, S., Briggs, D., Higgins, R., Khovanova, N.: Decision tree and random forest models for outcome prediction in antibody incompatible kidney transplantation. *Biomedical Signal Processing and Control* **52**, 456–462 (2019)
- [4] Yoo, D., Divard, G., Raynaud, M., Cohen, A., Mone, T.D., Rosenthal, J.T., Bentall, A.J., Stegall, M.D., Naesens, M., Zhang, H., Wang, C., Gueguen, J., Kamar, N., Bouquegneau, A., Batal, I., Coley, S.M., Gill, J.S., Oppenheimer, F., De Sousa-Amorim, E., Kuypers, D.R.J., Durrbach, A., Seron, D., Rabant, M., Van Huyen, J.-P.D., Campbell, P., Shojai, S., Mengel, M., Bestard, O., Basic-Jukic, N., Jurić, I., Boor, P., Cornell, L.D., Alexander, M.P., Toby Coates, P., Legendre, C., Reese, P.P., Lefaucheur, C., Aubert, O., Loupy, A.: A Machine Learning-Driven Virtual Biopsy System For Kidney Transplant Patients. *Nature Communications* **15**(1), 554 (2024) <https://doi.org/10.1038/s41467-023-44595-z>. Publisher: Nature Publishing Group. Accessed 2025-02-16
- [5] McKenney, C., Torabi, J., Todd, R., Akhtar, M.Z., Tedla, F.M., Shapiro, R., Florman, S.S., Holzner, M.L., van Leeuwen, L.L.: Wasted potential: Decoding the trifecta of donor kidney shortage, underutilization, and rising discard rates. *Transplantation* **5**(2), 51–64 (2024) <https://doi.org/10.3390/transplantation5020006>
- [6] Gotlieb, N., Azhie, A., Sharma, D., Spann, A., Suo, N.-J., Tran, J., Orchanian-Cheff, A., Wang, B., Goldenberg, A., Chassé, M., *et al.*: The promise of machine learning applications in solid organ transplantation. *NPJ digital medicine* **5**(1), 89 (2022)
- [7] Pettit, R.W., Marlatt, B.B., Miles, T.J., Uzgoren, S., Corr, S.J., Shetty, A., Havelka, J., Rana, A.: The utility of machine learning for predicting donor discard in abdominal transplantation. *Clinical transplantation* **37**(5), 14951 (2023) <https://doi.org/10.1111/ctr.14951>
- [8] Cucchetti, A., Vivarelli, M., Heaton, N.D., Phillips, S., Piscaglia, F., Bolondi, L., La Barba, G., Foxton, M.R., Rela, M., O’Grady, J., Pinna, A.D.: Artificial neural network is superior to meld in predicting mortality of patients with end-stage liver disease. *Gut* **56**(2), 253–258 (2007) <https://doi.org/10.1136/gut.2005.084434>
- [9] Zhou, S., Massie, A.B., Holscher, C.M., Waldram, M.M., Ishaque, T., Thomas, A.G., Segev, D.L.: Prospective Validation of Prediction Model for Kidney Discard. *Transplantation* **103**(4), 764–771 (2018) <https://doi.org/10.1097/tp.0000000000002362>
- [10] Massie, A.B., Desai, N.M., Montgomery, R.A., Singer, A.L., Segev, D.L.: Improving Distribution Efficiency of Hard-to-Place Deceased Donor Kidneys: Predicting Probability of Discard or Delay. *American Journal of Transplantation* **10**(7), 1613–1620 (2010) <https://doi.org/10.1111/j.1600-6143.2010.03163.x>
- [11] Marrero, W.J., Naik, A.S., Friedewald, J.J., Xu, Y., Hutton, D.W., Lavieri,

- M.S., Parikh, N.D.: Predictors of Deceased Donor Kidney Discard in the United States. *Transplantation* **101**(7), 1690–1697 (2016) <https://doi.org/10.1097/tp.0000000000001238>
- [12] Cohen, J.B., Shults, J., Goldberg, D.S., Abt, P.L., Sawinski, D.L., Reese, P.P.: Kidney allograft offers: Predictors of turndown and the impact of late organ acceptance on allograft survival. *American Journal of Transplantation* **18**(2), 391–401 (2017) <https://doi.org/10.1111/ajt.14449>
- [13] Narvaez, J.R.F., Nie, J., Noyes, K., Leeman, M., Kayler, L.K.: Hard-to-place kidney offers: Donor- and system-level predictors of discard. *American Journal of Transplantation* **18**(11), 2708–2718 (2018) <https://doi.org/10.1111/ajt.14712>
- [14] Barah, M., Mehrotra, S.: Predicting kidney discard using machine learning. *Transplantation* **105**(9), 2054–2071 (2021) <https://doi.org/10.1097/tp.0000000000003620>
- [15] Sageshima, J., Than, P., Goussous, N., Mineyev, N., Perez, R.: Prediction of High-Risk Donors for Kidney Discard and Nonrecovery Using Structured Donor Characteristics and Unstructured Donor Narratives. *JAMA Surgery* **159**(1), 60 (2023) <https://doi.org/10.1001/jamasurg.2023.4679>
- [16] Büyükkeçeci, M., Okur, M.C.: A comprehensive review of feature selection and feature selection stability in machine learning. *Gazi University Journal of Science* **36**(4), 1506–1520 (2023)
- [17] WHO, W.H.O.: ICD-10: International Statistical Classification of Diseases and Related Health Problems 10th Revision vol. 1, 5th edn. World Health Organization (WHO). <https://doi.org/10.1038/s41598-024-66976-0> . <https://apps.who.int/iris/bitstream/10665/246208/1/9789241549165-V1-eng.pdf>
- [18] Sauthier, N., Bouchakri, R., Carrier, F.M., Sauthier, M., Mullie, L.-A., Cardinal, H., Fortin, M.-C., Lahrichi, N., Chassé, M.: Automated screening of potential organ donors using a temporal machine learning model. *Scientific Reports* (2023) <https://doi.org/10.1038/s41598-023-35270-w>
- [19] Mohan, S., Husain, S.A., Schold, J.D., Reese, P.P., Stewart, D., Kadatz, M., Chow, D.S., Khurana, K.K., Axelrod, D., Mulligan, D.C., Formica, R.N., Roberts, J.P., Segev, D.L., Locke, J.E., Rees, M.J., Matas, A., Stegall, M.L., Cooper, M., Stock, P.G., Ellis, M.J., Heeger, P.S., Cohen, D.J., Danovitch, G.M., Montgomery, R.A., Bromberg, J.S., Redfield, R.R., Gaston, R.A., Gill, J., Kasiske, B.L., Kaplan, B.: A machine learning-driven virtual biopsy system for kidney transplantation. *Nature Communications* (2024) <https://doi.org/10.1038/s41467-023-44595-z>
- [20] Scikit-learn: IterativeImputer. (2024). Accessed: 2025-09-26. <https://scikit-learn.org/stable/modules/generated/sklearn.impute.IterativeImputer.html>

- [21] Scikit-learn: HistGradientBoostingClassifier. (2024). Accessed: 2025-03-29. <https://scikit-learn.org/stable/modules/generated/sklearn.ensemble.HistGradientBoostingClassifier.html>
- [22] Breiman, L., Friedman, J.H., Olshen, R.A., Stone, C.J.: Classification and Regression Trees. Chapman & Hall/CRC, Boca Raton and London and New York and Washington, D.C. (1984). <https://doi.org/10.1201/9781315139470> . <https://www.taylorfrancis.com/books/9781351460491>
- [23] Hosmer Jr, D.W., Lemeshow, S., Sturdivant, R.X.: Applied Logistic Regression. John Wiley & Sons
- [24] Breiman, L.: Random forests. Machine Learning **45**(1), 5–32 (2001) <https://doi.org/10.1023/A:1010933404324>
- [25] Chen, T., Guestrin, C.: Xgboost. In: Krishnapuram, B. (ed.) Proceedings of the 22nd ACM SIGKDD International Conference on Knowledge Discovery and Data Mining. ACM Digital Library, pp. 785–794. ACM, New York, NY (2016). <https://doi.org/10.1145/2939672.2939785>
- [26] Freund, Y., Schapire, R.E.: A decision-theoretic generalization of on-line learning and an application to boosting. Journal of computer and system sciences **55**(1), 119–139 (1997)
- [27] Wu, J., Li, Y., Ma, Y.: Comparison of xgboost and the neural network model on the class-balanced datasets. In: 2021 IEEE 3rd International Conference on Frontiers Technology of Information and Computer, pp. 457–461. IEEE, Piscataway, NJ (2021). <https://doi.org/10.1109/ICFTIC54370.2021.9647373>
- [28] Grinsztajn, L., Oyallon, E., Varoquaux, G.: Why do tree-based models still outperform deep learning on typical tabular data? Advances in neural information processing systems **35**, 507–520 (2022)
- [29] Goodfellow, I., Bengio, Y., Courville, A.: Deep Learning. MIT Press, ??? (2016). <http://www.deeplearningbook.org>
- [30] Holland, J.H.: Genetic algorithms. Scientific american **267**(1), 66–73 (1992)
- [31] Taha, Z.Y., Abdullah, A.A., Rashid, T.A.: Optimizing feature selection with genetic algorithms: a review of methods and applications. Knowledge and Information Systems, 1–40 (2025)
- [32] Liu, H., Setiono, R.: Feature selection and classification—a probabilistic wrapper approach. In: Industrial and Engineering Applications or Artificial Intelligence and Expert Systems, pp. 419–424. CRC Press
- [33] Ji, S., Carin, L.: Cost-sensitive feature acquisition and classification. Pattern

Recognition **40**(5), 1474–1485 (2007)

- [34] Deb, K., Pratap, A., Agarwal, S., Meyarivan, T.: A fast and elitist multiobjective genetic algorithm: Nsga-ii. *IEEE transactions on evolutionary computation* **6**(2), 182–197 (2002)
- [35] Hamano, R., Saito, S., Nomura, M., Shirakawa, S.: Cma-es with margin: Lower-bounding marginal probability for mixed-integer black-box optimization. In: *Proceedings of the Genetic and Evolutionary Computation Conference*, pp. 639–647 (2022)
- [36] Akiba, T., Sano, S., Yanase, T., Ohta, T., Koyama, M.: Optuna: A next-generation hyperparameter optimization framework. In: *Proceedings of the 25th ACM SIGKDD International Conference on Knowledge Discovery & Data Mining*, pp. 2623–2631 (2019)
- [37] Bergstra, J., Bengio, Y.: Random search for hyper-parameter optimization. *The journal of machine learning research* **13**(1), 281–305 (2012)
- [38] Matthews, B.W.: Comparison of the predicted and observed secondary structure of T4 phage lysozyme. *Biochimica et Biophysica Acta (BBA) - Protein Structure* **405**(2), 442–451 (1975) [https://doi.org/10.1016/0005-2795\(75\)90109-9](https://doi.org/10.1016/0005-2795(75)90109-9) . Accessed 2025-02-16
- [39] Chicco, D., Jurman, G.: The Matthews correlation coefficient (MCC) should replace the ROC AUC as the standard metric for assessing binary classification. *BioData Mining* **16**(1), 4 (2023) <https://doi.org/10.1186/s13040-023-00322-4> . Accessed 2025-02-16
- [40] Chicco, D., Jurman, G.: The advantages of the Matthews correlation coefficient (MCC) over F1 score and accuracy in binary classification evaluation. *BMC Genomics* **21**(1), 6 (2020) <https://doi.org/10.1186/s12864-019-6413-7> . Accessed 2025-02-16
- [41] Atallah, D.M., Badawy, M., El-Sayed, A.: Intelligent feature selection with modified k-nearest neighbor for kidney transplantation prediction. *SN Applied Sciences* **1**(10), 1297 (2019)
- [42] Chen, Y., Gao, J., Wu, J.: Dynamic feature selection in medical predictive monitoring by reinforcement learning. *arXiv preprint arXiv:2405.19729* (2024)
- [43] Bergstra, J., Bardenet, R., Bengio, Y., Kégl, B.: Algorithms for hyper-parameter optimization. *Advances in neural information processing systems* **24** (2011)
- [44] Turner, R., Eriksson, D., McCourt, M., Kiili, J., Laaksonen, E., Xu, Z., Guyon, I.: Bayesian optimization is superior to random search for machine learning hyper-parameter tuning: Analysis of the black-box optimization challenge 2020. In:

NeurIPS 2020 Competition and Demonstration Track, pp. 3–26 (2021). PMLR

- [45] Hollmann, N., Müller, S., Eggenberger, K., Hutter, F.: TabPFN: A transformer that solves small tabular classification problems in a second. arXiv preprint arXiv:2207.01848 (2022)
- [46] Bardes, A., Ponce, J., LeCun, Y.: Vicreg: Variance-invariance-covariance regularization for self-supervised learning. arXiv preprint arXiv:2105.04906 (2021)
- [47] Gorishniy, Y.V., Rubachev, I., Khrulkov, V., Babenko, A.: Revisiting deep learning models for tabular data. ArXiv **abs/2106.11959** (2021)
- [48] Defazio, A., Bach, F., Lacoste-Julien, S.: Saga: A fast incremental gradient method with support for non-strongly convex composite objectives. *Advances in neural information processing systems* **27** (2014)
- [49] Breiman, L.: Bagging predictors. *Machine learning* **24**(2), 123–140 (1996)
- [50] Glorot, X., Bengio, Y.: Understanding the difficulty of training deep feedforward neural networks. In: *Proceedings of the Thirteenth International Conference on Artificial Intelligence and Statistics*, pp. 249–256 (2010). JMLR Workshop and Conference Proceedings
- [51] He, K., Zhang, X., Ren, S., Sun, J.: Delving deep into rectifiers: Surpassing human-level performance on imagenet classification. In: *Proceedings of the IEEE International Conference on Computer Vision*, pp. 1026–1034 (2015)
- [52] Desai, C., Desai, C.: Impact of weight initialization techniques on neural network efficiency and performance: a case study with mnist dataset. *International Journal Of Engineering And Computer Science* **13**(04) (2024)
- [53] Christen, P., Hand, D.J., Kirielle, N.: A review of the f-measure: its history, properties, criticism, and alternatives. *ACM Computing Surveys* **56**(3), 1–24 (2023)
- [54] Hanley, J.A., McNeil, B.J.: The meaning and use of the area under a receiver operating characteristic (roc) curve. *Radiology* **143**(1), 29–36 (1982)
- [55] Hanczar, B., Hua, J., Sima, C., Weinstein, J., Bittner, M., Dougherty, E.R.: Small-sample precision of roc-related estimates. *Bioinformatics* **26**(6), 822–830 (2010)
- [56] Lobo, J.M., Jiménez-Valverde, A., Real, R.: Auc: a misleading measure of the performance of predictive distribution models. *Global ecology and Biogeography* **17**(2), 145–151 (2008)
- [57] Girden, E.R.: ANOVA: Repeated Measures vol. 84. sage

- [58] Nanda, A., Mohapatra, B.B., Mahapatra, A.P.K., Mahapatra, A.P.K., Mahapatra, A.P.K.: Multiple comparison test by tukey’s honestly significant difference (hsd): Do the confident level control type i error. *International Journal of Statistics and Applied Mathematics* **6**(1), 59–65 (2021)
- [59] Haller, M.C., Aschauer, C., Wallisch, C., Leffondré, K., Smeden, M., Oberbauer, R., Heinze, G.: Prediction models for living organ transplantation are poorly developed, reported, and validated: a systematic review. *Journal of Clinical Epidemiology* **145**, 126–135 (2022)
- [60] Ali, H., Shroff, A., Fülöp, T., Molnar, M.Z., Sharif, A., Burke, B., Shroff, S., Briggs, D., Krishnan, N.: Artificial intelligence assisted risk prediction in organ transplantation: a uk live-donor kidney transplant outcome prediction tool. *Renal Failure* **47**(1), 2431147 (2025)
- [61] Salaün, A., Knight, S., Wingfield, L., Zhu, T.: Predicting graft and patient outcomes following kidney transplantation using interpretable machine learning models. *Scientific Reports* **14**(1), 17356 (2024)
- [62] Brier, G.W., Allen, R.A.: Verification of weather forecasts. In: *Compendium of Meteorology: Prepared Under the Direction of the Committee on the Compendium of Meteorology*, pp. 841–848. Springer
- [63] Murphy, A.H.: A new vector partition of the probability score. *Journal of Applied Meteorology and Climatology* **12**(4), 595–600 (1973)
- [64] Ojeda, F.M., Jansen, M.L., Thiéry, A., Blankenberg, S., Weimar, C., Schmid, M., Ziegler, A.: Calibrating machine learning approaches for probability estimation: A comprehensive comparison. *Statistics in medicine* **42**(29), 5451–5478 (2023) <https://doi.org/10.1002/sim.9921>
- [65] Rufibach, K.: Use of brier score to assess binary predictions. *Journal of clinical epidemiology* **63**(8), 938–939 (2010)
- [66] Platt, J., *et al.*: Probabilistic outputs for support vector machines and comparisons to regularized likelihood methods. *Advances in large margin classifiers* **10**(3), 61–74 (1999)
- [67] Zadrozny, B., Elkan, C.: Transforming classifier scores into accurate multiclass probability estimates. In: *Proceedings of the Eighth ACM SIGKDD International Conference on Knowledge Discovery and Data Mining*, pp. 694–699 (2002)
- [68] Lundberg, S., Lee, S.-I.: A Unified Approach to Interpreting Model Predictions. *arXiv. arXiv:1705.07874 [cs]* (2017). <https://doi.org/10.48550/arXiv.1705.07874> . <http://arxiv.org/abs/1705.07874> Accessed 2025-02-20
- [69] Shapley, L.S.: A value for n-person games. *Contribution to the Theory of Games*

- [70] Zheng, Q., Wang, Z., Zhou, J., Lu, J.: Shap-cam: Visual explanations for convolutional neural networks based on shapley value. In: European Conference on Computer Vision, pp. 459–474 (2022). Springer
- [71] Mosca, E., Szigeti, F., Tragianni, S., Gallagher, D., Groh, G.: Shap-based explanation methods: a review for nlp interpretability. In: Proceedings of the 29th International Conference on Computational Linguistics, pp. 4593–4603 (2022)
- [72] Rodríguez-Pérez, R., Bajorath, J.: Interpretation of machine learning models using shapley values: application to compound potency and multi-target activity predictions. *Journal of computer-aided molecular design* **34**(10), 1013–1026 (2020)
- [73] Saarela, M., Jauhiainen, S.: Comparison of feature importance measures as explanations for classification models. *SN Applied Sciences* **3**(2), 272 (2021)
- [74] Saeed, W., Omlin, C.: Explainable AI (XAI): A systematic meta-survey of current challenges and future opportunities. *Knowledge-Based Systems* **263**, 110273 (2023) <https://doi.org/10.1016/j.knosys.2023.110273> . Accessed 2025-03-19
- [75] Scholbeck, C.A., Molnar, C., Heumann, C., Bischl, B., Casalicchio, G.: Sampling, intervention, prediction, aggregation: a generalized framework for model-agnostic interpretations. In: Machine Learning and Knowledge Discovery in Databases: International Workshops of ECML PKDD 2019, Würzburg, Germany, September 16–20, 2019, Proceedings, Part I, pp. 205–216 (2020). Springer
- [76] Decruyenaere, A., Decruyenaere, P., Peeters, P., Vermassen, F., Dhaene, T., Couckuyt, I.: Prediction of delayed graft function after kidney transplantation: comparison between logistic regression and machine learning methods. *BMC medical informatics and decision making* **15**(1), 83 (2015)
- [77] Esmaily, H., Tayefi, M., Doosti, H., Ghayour-Mobarhan, M., Nezami, H., Amirabadizadeh, A.: A comparison between decision tree and random forest in determining the risk factors associated with type 2 diabetes. *Journal of research in health sciences* **18**(2), 412 (2018)
- [78] Slonim, D.K.: From patterns to pathways: gene expression data analysis comes of age. *Nature genetics* **32**(4), 502–508 (2002)
- [79] Tolstyak, Y., Zhuk, R., Yakovlev, I., Shakhovska, N., Gregus ml, M., Chopyak, V., Melnykova, N.: The Ensembles of Machine Learning Methods for Survival Predicting after Kidney Transplantation. *Applied Sciences* **11**(21), 10380 (2021) <https://doi.org/10.3390/app112110380> . Number: 21 Publisher: Multidisciplinary Digital Publishing Institute. Accessed 2025-02-16

- [80] Reeve, J., Böhmig, G.A., Eskandary, F., Einecke, G., Gupta, G., Madill-Thomsen, K., Mackova, M., Halloran, P.F., INTERCOMEX MMDx-Kidney Study Group: Generating automated kidney transplant biopsy reports combining molecular measurements with ensembles of machine learning classifiers. *American Journal of Transplantation: Official Journal of the American Society of Transplantation and the American Society of Transplant Surgeons* **19**(10), 2719–2731 (2019) <https://doi.org/10.1111/ajt.15351>
- [81] Wilks, D.S.: On the combination of forecast probabilities for consecutive precipitation periods. *Weather and forecasting* **5**(4), 640–650 (1990)
- [82] Wüthrich, M.V., Merz, M.: *Statistical Foundations of Actuarial Learning and Its Applications*. Springer
- [83] Niculescu-Mizil, A., Caruana, R.: Predicting good probabilities with supervised learning. In: Džeroski, S. (ed.) *Proceedings of the 22nd International Conference on Machine Learning*. ACM Other conferences, pp. 625–632. ACM, New York, NY (2005). <https://doi.org/10.1145/1102351.1102430>
- [84] Guo, C., Pleiss, G., Sun, Y., Weinberger, K.Q.: On calibration of modern neural networks. In: *International Conference on Machine Learning*, pp. 1321–1330 (2017). PMLR
- [85] Sageshima, J., Than, P., Goussous, N., Mineyev, N., Perez, R.: Prediction of high-risk donors for kidney discard and nonrecovery using structured donor characteristics and unstructured donor narratives. *JAMA surgery* **159**(1), 60–68 (2024)
- [86] Sauthier, N., Bouchakri, R., Carrier, F.M., Sauthier, M., Mullie, L.-A., Cardinal, H., Fortin, M.-C., Lahrichi, N., Chassé, M.: Automated screening of potential organ donors using a temporal machine learning model. *Scientific Reports* **13**(1), 8459 (2023)
- [87] Shiri, F.M., Perumal, T., Mustapha, N., Mohamed, R.: A comprehensive overview and comparative analysis on deep learning models: Cnn, rnn, lstm, gru. *arXiv preprint arXiv:2305.17473* (2023)
- [88] Noor, M.H.M., Ige, A.O.: A survey on state-of-the-art deep learning applications and challenges. *Engineering Applications of Artificial Intelligence* **159**, 111225 (2025)
- [89] Borisov, V., Leemann, T., Seßler, K., Haug, J., Pawelczyk, M., Kasneci, G.: Deep neural networks and tabular data: A survey. *IEEE transactions on neural networks and learning systems* **35**(6), 7499–7519 (2022)
- [90] Huang, X., Marques-Silva, J.: On the failings of shapley values for explainability. *International Journal of Approximate Reasoning* **171**, 109112 (2024)

- [91] Kumar, I., Scheidegger, C., Venkatasubramanian, S., Friedler, S.: Shapley residuals: Quantifying the limits of the shapley value for explanations. *Advances in Neural Information Processing Systems* **34**, 26598–26608 (2021)
- [92] Pedregosa, F., Varoquaux, G., Gramfort, A., Michel, V., Thirion, B., Grisel, O., Blondel, M., Prettenhofer, P., Weiss, R., Dubourg, V., Vanderplas, J., Passos, A., Cournapeau, D., Brucher, M., Perrot, M., Duchesnay, E.: Scikit-learn: Machine learning in Python. *Journal of Machine Learning Research* **12**, 2825–2830 (2011)
- [93] Paszke, A., Gross, S., Massa, F., Lerer, A., Bradbury, J., Chanan, G., Killeen, T., Lin, Z., Gimelshein, N., Antiga, L., et al.: Pytorch: An imperative style, high-performance deep learning library. *Advances in neural information processing systems* **32** (2019)

Supplementary information.

Appendix A Software and Hardware

We use an AMD EPYC-Milan Processor for all models trained with sklearn [92] version 1.5.2 (Decision Tree, Random Forest, Logistic Regression) and xgboost version 2.1.2. We train our MLP models with pytorch [93] version 2.5.0 and cuda version 12.2 on a NVIDIA A100 Graphic card. We use the shap package [68] version 0.46.0 for explainability.

Appendix B Feature Engineering

B.1 Feature Transformations

- **Age at Diabetes Diagnosis** The donor’s age at the time of the diabetes diagnosis is calculated using the timestamps of their birth and the diagnosis date.
- **Duration of Diabetes** The duration of diabetes for the donor is calculated using the timestamps of the diagnosis and the time of death.
- **Duration of Alcohol Consumption** The calculation of this feature depends on whether an end is provided for the respective donor. If an end date is available, the duration of alcohol consumption (in days) is computed as the difference between the start and end dates. If no end date is provided, it is assumed that the date of hospital admission represents the end point for that donor.
- **Last Alcohol Consumption** This feature categorically represents the time elapsed since a donor’s last alcohol consumption. The categorization is based on the difference between the documented end of alcohol use and the date of hospital admission. The calculation is performed as follows:
 - No alcohol consumption documented: If no start date for alcohol consumption is provided, it is assumed that the donor does not have an alcohol-related issue and is assigned to category 0.

- Currently consuming: If a start date is available but no end date is given, it is assumed that the donor was consuming up until hospital admission. In this case, the time difference is 0 days, and the donor is assigned to the highest category, category 5.
- Consumption ended prior to admission: If both a start and end date are available, the number of days between the end of alcohol use and hospital admission is calculated. This time span is then divided into four categories. The bins are determined dynamically based on the distribution in the training dataset, where donors who stopped drinking more recently fall into higher categories (e.g. category 4), and those whose last consumption was further in the past are placed in lower categories (e.g. category 1).
- For some categorical variables with rare values we grouped values into positive and negative to turn them into binary features, e.g. "EKG result on QRS differences" was dichotomized into "no" if no differences are reported and "yes" if "others", "MI-like", "RSB", "LSB" or "bifascicular block" is reported.
- The amount of diuresis in the last hour (dlh) was normalized using body weight (bw) (see formula B1).
- The total amount of diuresis (dt) within a time window (t) was scaled to 24 hours and normalized to body weight (see formula B2)
- We converted creatinine values to the unit mg/dL, by multiplying the values by a factor of 0.011312 (given in $\mu mol/L$ in the primary database).

$$dlh_{norm} = \frac{dlh}{bw} \tag{B1}$$

$$d_{24h/bw} = \frac{dt}{t \text{ (in hours)}} \cdot \frac{24}{bw} \tag{B2}$$

Appendix C Hyperparameter Results

C.1 Hyperparameter Spaces

	mean	std	min	25%	50%	75%	max
max depth	17.19667	11.33016	1	8	15	24	49
min samples leaf	13.67667	4.15246	1	12	14	16	20
min samples split	9.70333	5.67120	2	5	8	15	20

Table C1 Summary Statistics of Decision Tree Hyperparameter search: Mean, Standard Deviation, Minimum, and Maximum Values for Max Depth, Minimum Samples Leaf, and Minimum Samples Split from 300 trials.

	mean	std	min	25%	50%	75%	max
C	12.03738	20.69000	0.01497	0.59561	2.10518	15.78112	97.24803
l1 ratio	0.77262	0.20096	0.00505	0.70081	0.81645	0.91059	0.99963

Table C2 Summary Statistics of Logistic Regression Hyperparameter search: Mean, Standard Deviation, Minimum, and Maximum Values for C and l1 ratio from 300 trials.

	mean	std	min	25%	50%	75%	max
max depth	28.70333	11.99032	1	20	30	37	50
min samples leaf	7.69667	4.11352	1	5	7	9	20
min samples split	15.90667	5.05931	2	15	18	20	20
n estimators	393.70333	130.46514	10	367.75000	445.50000	484	500

Table C3 Summary Statistics of Random Forest Hyperparameter search: Mean, Standard Deviation, Minimum, and Maximum Values for n estimators, Max Depth, Minimum Samples Leaf, and Minimum Samples Split from 300 trials.

	mean	std	min	25%	50%	75%	max
colsample bytree	0.80872	0.05063	0.75021	0.76957	0.79353	0.83285	0.99825
early stopping rounds	44.51667	27.23028	5	20	45	65	100
learning rate	0.02292	0.02188	0.00108	0.00856	0.01462	0.03076	0.09703
max depth	4.74000	2.92591	2	3	4	6	15
min child weight	11.76333	5.77626	1	6	13	17	20
n estimators	1013.66667	414.85367	100	700	1150	1350	1500
reg alpha	0.54814	2.13458	0.00103	0.00491	0.02079	0.13249	19.89581
reg lambda	0.87691	3.01173	0.00102	0.00361	0.02605	0.21597	22.85764
subsample	0.90318	0.07581	0.75181	0.84068	0.92029	0.97013	0.99973

Table C4 Summary Statistics of XGB Hyperparameter search: Mean, Standard Deviation, Minimum, and Maximum Values for colsample bytree, early stopping rounds, learning rate, max depth, min child weight, n estimators, reg alpha/lambda, and subsample from 300 trials.

	mean	std	min	25%	50%	75%	max
batchnorm	0.766667	0.423659	0	1	1	1	1
dropout	0.367333	0.113398	0	0.300000	0.400000	0.450000	0.500000
hidden dim	838.613333	350.107032	1010	5800	8580	1065.250000	15000
init lr	0.002675	0.010163	0.000100	0.000145	0.000255	0.000677	0.090003
n layer	4.676667	2.948633	20	30	40	60	150
weight decay	$1.009 \times e^{-7}$	$2.1 \times e^{-7}$	$1.002 \times e^{-10}$	$2.34 \times e^{-10}$	$1.9 \times e^{-9}$	$7.02 \times e^{-8}$	$9.91 \times e^{-7}$

Table C5 Summary Statistics of MLP Hyperparameter search: Mean, Standard Deviation, Minimum, and Maximum Values for batchnorm (use or not), dropout probability, hidden dimension, initial learning rate, and weight decay from 300 trials.

Hyperparameter	Value
max depth	7
max features	sqrt
min samples leaf	18
min samples split	15

Table C6 Best Decision Tree Configuration from Hyperparameter Search

Hyperparameter	Value
C	0.07085
l1 ratio	0.88392

Table C7 Best Logistic Regression Configuration from Hyperparameter Search

Hyperparameter	Value
max depth	7
max features	sqrt
min samples leaf	18
min samples split	15

Table C8 Best Random Forest Configuration from Hyperparameter Search

Hyperparameter	Value
colsample bytree	0.80955
early stopping rounds	75
learning rate	0.01551
max depth	3
min child weight	4
n estimators	1300
reg alpha	0.01442
reg lambda	2.46270
subsample	0.99142
tree method	hist

Table C9 Best XGB Configuration from Hyperparameter Search

Hyperparameter	Value
activation function	ELU
batchnorm	1
class weights	0
dropout	0.35000
hidden dim	1121
init lr	0.00012
n layer	3
weight decay	$1 \times e^{-10}$

Table C10 Best MLP Configuration from Hyperparameter Search

C.2 Final Architectures

Appendix D Further Tukey Results

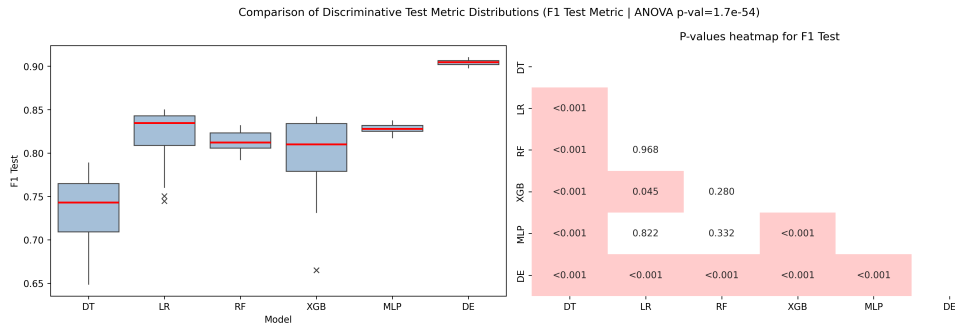


Fig. D1 Left: Discrimination performance evaluation of six different Machine Learning models. Each panel reports the test F1 Score (Y-axis, higher is better) for multiple approaches: XGB, RF, MLP, LR, DT, and DE. Boxplots show the performance distribution for each method. **Right:** Lower-triangle heatmap of Tukey-adjusted p-values showing pairwise statistical significance between models.

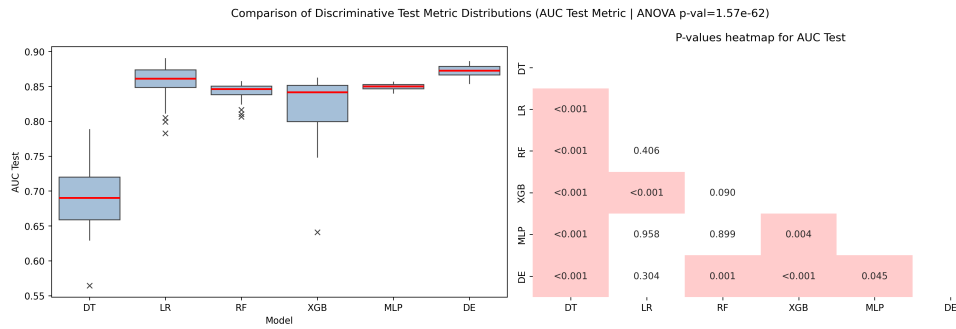


Fig. D2 Left: Discrimination performance evaluation of six different Machine Learning models. Each panel reports the test AUC (Y-axis, higher is better) for multiple approaches: XGB, RF, MLP, LR, DT, and DE. Boxplots show the performance distribution for each method. **Right:** Lower-triangle heatmap of Tukey-adjusted p-values showing pairwise statistical significance between models.

Appendix E Calibration

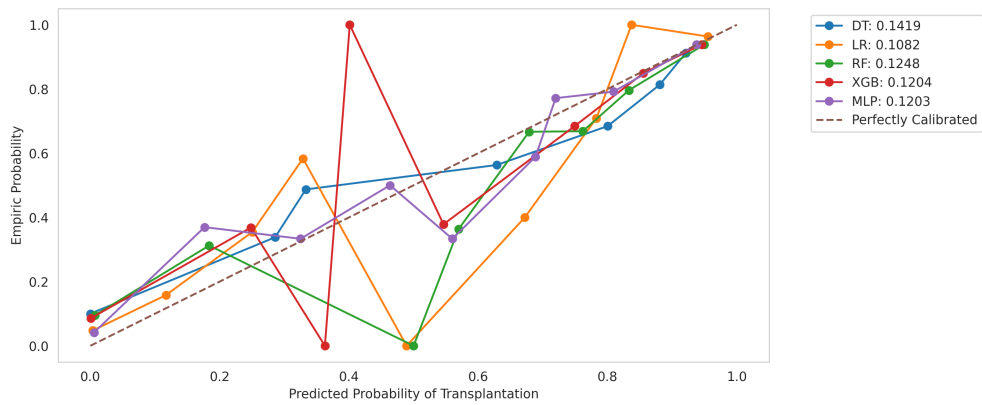


Fig. E3 Calibration curves for isotonic calibration for DT, RF, LR, XGB, and MLP.

Appendix F Explainability

F.1 Logistic Regression

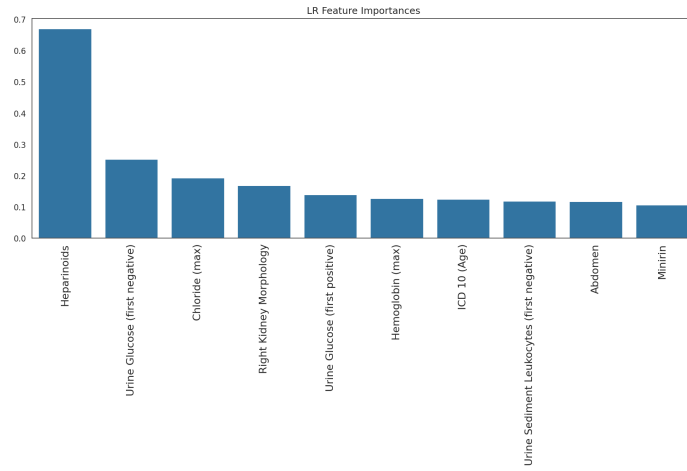


Fig. F4 Model-specific explainability via LR coefficients (y-axis), highlighting top features such as time-series aggregates of renal function measures and medication information.

F.2 Decision Tree

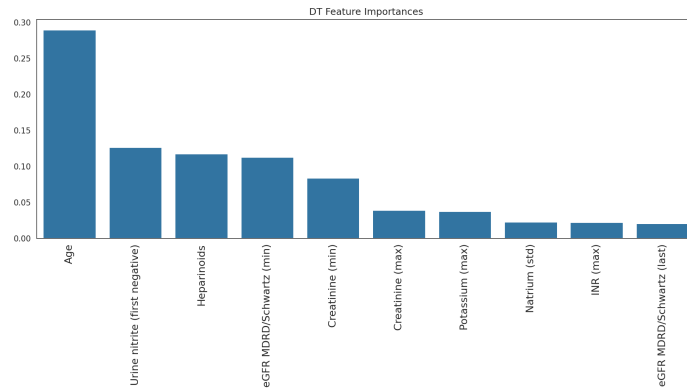


Fig. F5 Model-specific explainability via DT feature importance (y-axis), highlighting top features such as time-series aggregates of renal function measures and medication information.

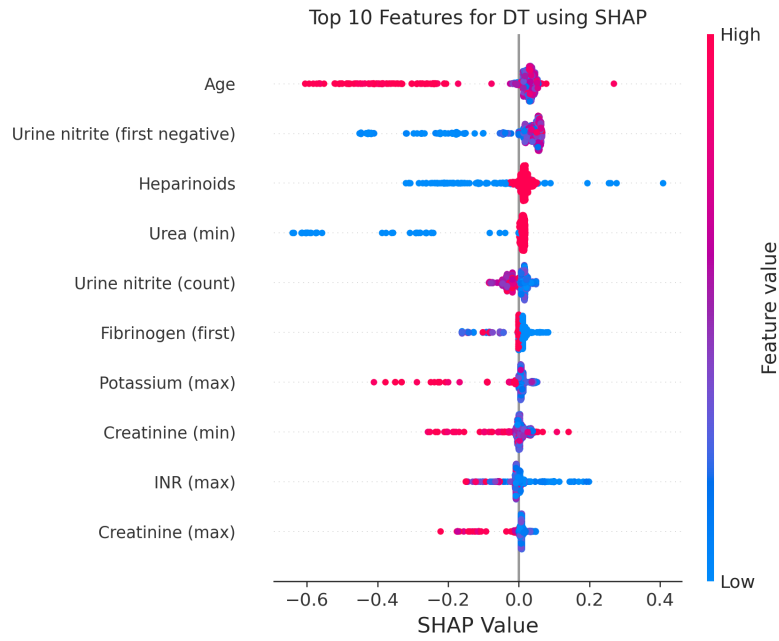


Fig. F6 Beeswarm plot of SHAP values showing the distribution and impact of features on DT donor transplantation predictions. Each point represents an individual instance (test set), positioned by its SHAP value and colored by the feature's actual value, illustrating both the magnitude and direction of feature influence. Top features include age, time-series aggregates of renal function measures and medication information.

F.3 Random Forest

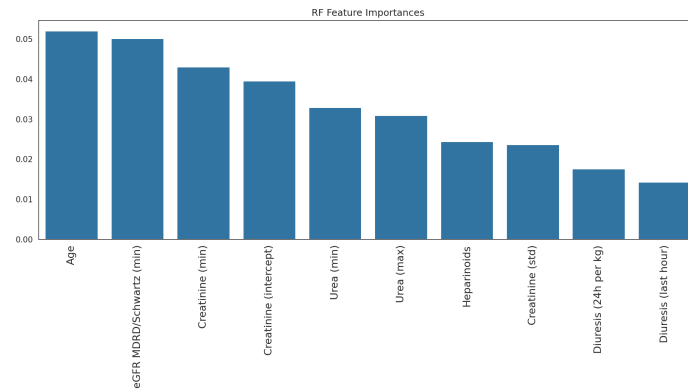


Fig. F7 Model-specific explainability via RF feature importance (y-axis), highlighting top features such as age, time-series aggregates of renal function measures and medication information.

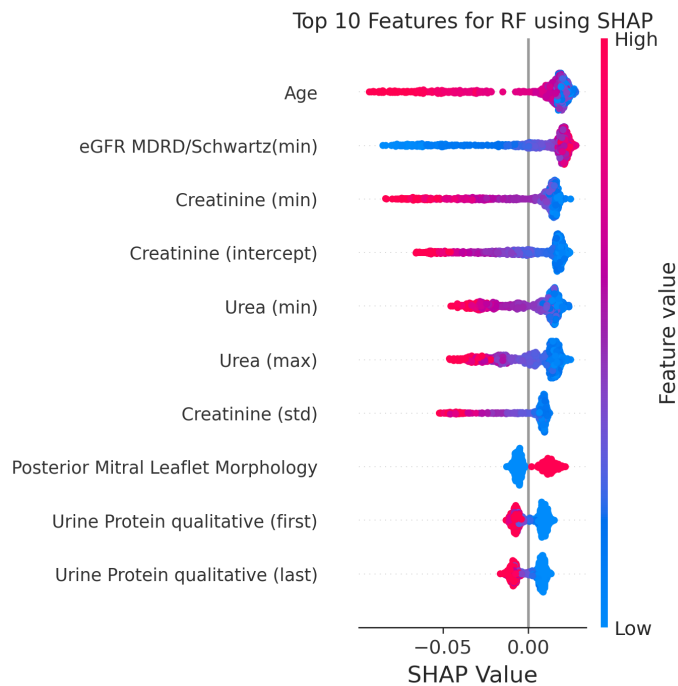


Fig. F8 Beeswarm plot of SHAP values showing the distribution and impact of features on RF donor transplantation predictions. Each point represents an individual instance (test set), positioned by its SHAP value and colored by the feature's actual value, illustrating both the magnitude and direction of feature influence. Top features include age, time-series aggregates of renal function measures and medication information.

F.4 XGB

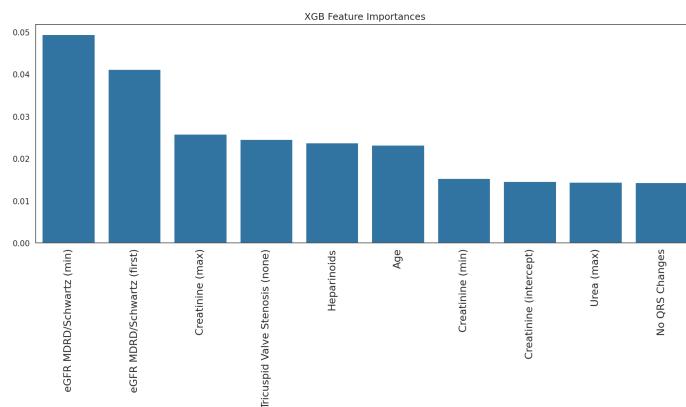


Fig. F9 Model-specific explainability via XGB feature importance (y-axis), highlighting top features such as age, time-series aggregates of renal function measures and medication information.

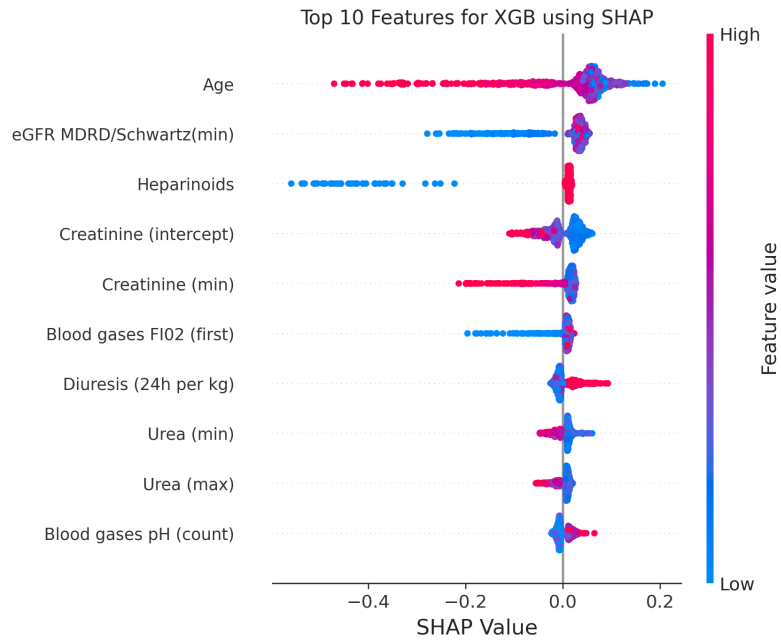


Fig. F10 Beeswarm plot of SHAP values showing the distribution and impact of features on XGB donor transplantation predictions. Each point represents an individual instance (test set), positioned by its SHAP value and colored by the feature's actual value, illustrating both the magnitude and direction of feature influence. Top features include age, time-series aggregates of renal function measures and medication information.

F.5 MLP

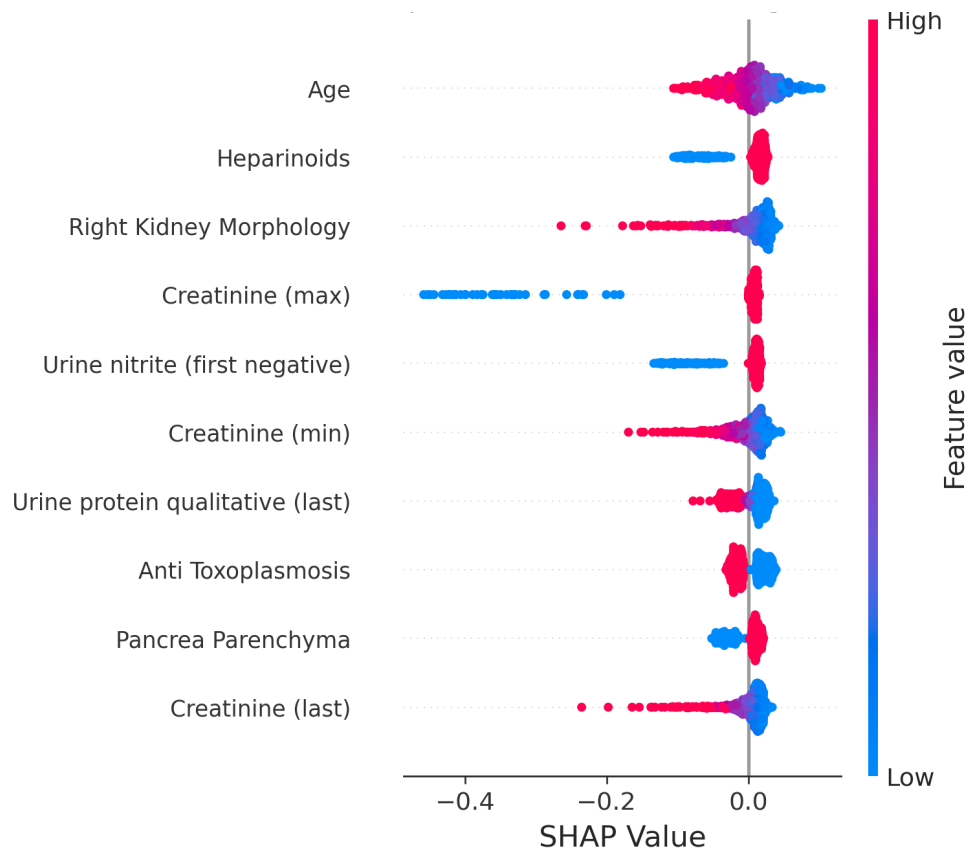


Fig. F11 Beeswarm plot of SHAP values showing the distribution and impact of features on MLP donor transplantation predictions. Each point represents an individual instance (test set), positioned by its SHAP value and colored by the feature's actual value, illustrating both the magnitude and direction of feature influence. Top features include age, time-series aggregates of renal function measures and medication information.